Morphology of Ionic Aggregates in Carboxylato- and Sulfonato-Telechelic Polyisoprenes As Investigated by Small-Angle X-ray Scattering

Roger Sobry,*,† Frédéric Fontaine,† Jean Ledent,† Marianne Foucart,‡ and Robert Jérôme‡

Laboratory of Experimental Physics, Institute of Physics B5, University of Liège, B−4000 Liège, Belgium, and Center for Education and Research on Macromolecules (CERM), Institute of Chemistry B6, University of Liège, B-4000 Liège, Belgium

Received January 22, 1997; Revised Manuscript Received December 1, 1997

ABSTRACT: Twenty seven samples of carboxylato- and sulfonato-telechelic polyisoprenes associated with various cations (Na, K, Rb, Cs, Mg, Ca, Sr, and Ba) have been investigated by small-angle X-ray scattering. The Bragg spacing characteristic of the ionic peak is directly proportional to the root-mean-square end-to-end distance (r_{rms}) of the polyisoprene chain. In the series of sulfonato-telechelic polyisoprenes, the Bragg spacing is approximately equal to r_{rms}, whereas in the series of carboxylato-telechelic polyisoprenes it amounts to $2^{1/2}\, r_{rms}$. It also appears that the ionic aggregates are more likely distributed according to a planar hexagonal network. An original method has been used for the tail-end analysis of the SAXS profile, which is based on the general vertex contribution to the Kirste−Porod law. It results that the ionic aggregates are of an angulous shape. Four different functions have been used to account for the interphase profile between the ionic phase and the polymeric matrix. The ionic aggregates would accordingly contain an average of 10 alkali-metal cations with a tetrahedral stacking, whereas six alkaline-earth-metal cations would be organized according to an equilateral prism. The oxygen atoms of the anionic groups mainly contribute to the width of the interface. The additional peaks observed in the upturn of the curve at very low angles are the signature of a superstructure similar to that one previously observed for carboxylato-telechelic poly(*tert*-butyl acrylate)s.

Introduction

The thermomechanical properties of hydrophobic polymers are deeply modified by the random covalent bonding of less than 15 mol % ionic groups. Although these polymers known as ionomers have been extensively studied, it is still quite a problem to clear up the fundamental structure−property relationhips. Eisenberg[1] was the first to propose a model for the morphology of ionomers. Steric and energetic arguments led him to propose that the ion pairs tend to associate into multiplets, which, above a critical ion pair concentration, loosely associate into clusters. There was a long debate about the nature and structure of multiplets and clusters.[2] Recently, the original multiplet-cluster model has been revised by Eisenberg et al.[3] on the assumption that each multiplet is surrounded by a region of restricted mobility, which above the critical ion content starts to overlap and to form domains large enough to exhibit a characteristic glass transition temperature. The ionomer is then a typical two-phase system. The assumption of a local restriction in the segmental chain mobility of ionomers has recently been supported by NMR experiments.[4,5]

Halato-telechelic polymers (HTP's) have been designed as model ionomers which consist of short linear chains selectively terminated by an ionic group at both ends.[6] The network junction points are then located at the chain ends and thus separated by a well-defined distance which can be varied as desired.

Small-angle X-ray and neutron scattering has provided the most convincing evidence for a microphase separation in ionomers as result of a large difference in polarity between the salt groups and the hydrophobic polymer matrix. A well-defined peak in the SAXS profile is usually observed and referred to as the "ionic peak". The peak position corresponds to a Bragg spacing of a few nanometers (2−12 nm) for both HTP's[7,8] and ionomers.[9−11] Although all the models that have been proposed to account for the SAXS data refer to multiplets as the basic scattering units, they do not agree on the assignment of the ionic peak which might result from either interparticule interference or the internal structure of noninteracting particles (intraparticle interference).

Another characteristic feature of the SAXS profiles of ionomers and HTP's has to be found in a strong upturn in intensity in the Guinier region.[7,8,12−17] The available models[12−15] do not however predict this intensity upturn at very low angles. Its origin has been tentatively assigned to large size heterogeneities and more particulaly to isolated ion-pairs inhomogeneously distributed throughout the polymer matrix.[17−23]

This paper aims at reporting on a systematic study of α,ω-metal sulfonato and carboxylato polyisoprenes by SAXS. Various cations have been used (Ba, Mg, Ca, Sr, K, Cs, Na and Rb) and the chain molecular weight, M_n, has been varied in the range 5000−21000. Particular attention has also been paid to the degree of neutralization of the acid end groups.

Three major issues will be discussed in this paper. First the analysis of the SAXS data, particularly the analysis of the tail-end of the curve, will be briefly

† Institute of Physics B5.
‡ Institute of Chemistry B6.

S0024-9297(97)00065-X CCC: $15.00
Published on Web 06/06/1998

revised with the purpose to take into account both the positive and negative deviations from the well-known asymptotic Porod law. The negative deviations that result from a diffuse interface will be examined in reference to different interface models based on different electronic density profiles. Contribution of the Kirste−Porod term to the asymptotic law will be considered and its physical meaning discussed. The second section will deal with the dependence of the ionic peak position on the chain molecular weight, the structureof the ion pair, the degree of neutralization of the acid end groups, and the nature of the polymer backbone. Diffusion at very small angles will be discussed in relation to a possible superstructure promoted by the distribution of the ionic aggregates. The last section will be concerned with the tail-end analysis of the SAXS data, and a general model will be proposed for the aggregation of the ionic groups.

Experimental Section

α,ω-carboxylic acid and sulfonic acid polyisoprenes were synthesized by the living anionic polymerization of isoprene initiated by a dianion and terminated by CO_2 and propanesultone, respectively. Carboxylic acid and sulfonic acid endgroups were quantitatively neutralized with stoiechiometric amounts of metal alkoxides and metal acetates, respectively, as reported elsewhere.[24] Molecular weight (and molecular weight distribution) were measured by size exclusion chromatography, with calibration with polystyrene standards.

Samples for SAXS experiments were molded at high temperature (420 K) and rapidly cooled so that organization cannot occur during the sample preparation.[25]

SAXS intensities were measured with a Kratky compact camera and a traditional stabilized X-ray generator (Cu Kα radiation) equipped with a Ni β-filter and a pulse height discriminator. The scattered intensity was registered with a Xe-filled high-efficiency Philips counter. The fixed time mode was currently used with a sampling time of 200 s per step. At very small angles where the intensity was high enough, the fixed count mode was however used at a rate of 100 000 counts per step. Absorption, sample thickness, parasitic scattering and electronic noise were taken into account in the standard manner.[26] The entrance and detector slits were 100 and 250 μm, respectively. However, the first part of the curve at the smallest angles was also registered with an entrance and a detector slit of 50 and 125 μm, respectively, and then multiplied by a scaling factor to merge both registered curves. The explored angular domain was $0.0008 = 2\ \theta = 0.15$ rad (i.e., $0.045° = 2\theta = 8.5°$; $0.005 = s = 1\ nm^{-1}$), corresponding to about 250 steps per sample.

SAXS Data Treatment: Deviations from the Ideal Porod Law. The background of the SAXS curves is generally small for most the studied polyisoprene samples and a background of the B_2s^2 form is quite an acceptable approximation, B_2 being a constant. The background was subtracted from the experimental intensity.

Desmearing of the SAXS curves registered in the finite slit mode was carried out by the Vonk method [26] and by an original method reported by Sobry et al.[27] The latter method [27] is based on the fitting of the tail end of the experimental smeared curve with a theoretical Porod law, taking into account the finite thickness of the interphase as proposed by Koberstein et al.[28] Briefly, for large s values, the pinhole intensity may be written as

$$I = I_P(s)H^2(\sigma,s) \tag{1}$$

where $s = (2 \sin \theta)/\lambda$, θ is the half-scattering angle, λ is the wavelength of the incident radiation, $I_P(s) = K_P/s^4$ is the Porod intensity, and K_P is a constant. The Porod intensity, I_P, is only valid for an ideal system with sharp interfaces between the phases, and the broadening function, $H^2(\sigma,s)$, depends on the shape and width (σ) of the interphase.

In the case of a linearly decreasing electronic density between the phases

$$H(\sigma,s) = \sin x/x \quad \text{(Vonk function,[28,29] abbreviated as } V)$$

where $x = \pi 12^{1/2}\sigma s$. If the electronic density profile were sigmoidal, then H(σ, s) would be a Gaussian function:

$$H(\sigma,s) = \exp(-2\pi^2\sigma^2s^2)$$

(Gaussian function,[28,30] denoted as G)

From the thermodynamics of the electronic density profile, the results

$$H(\sigma,s) = x \operatorname{cosech} x \quad \text{(Roe function,[31] noted as } R)$$

is obtained. The three $H^2(\sigma,s)$ functions are quite similar as long as s is not exceedingly large, and they also have the same Mac Laurin expansion when σs is small (eq 2). Equation 2 is

$$H^2(\sigma,s) \approx 1 - 4\pi^2\sigma^2s^2 \tag{2}$$

linear in s^2 and denoted L. It is often used instead of the more accurate G, V, or R functions in which σ is clearly the standard deviation of the electronic density profile in the real space. $E = 12^{1/2}\ \sigma$ is usually considered as the half-width of the electronic density fluctuation at the phase separation. Koberstein et al.[28] have argued that the use of the approximation L rather than functions G or V yields underestimated σ values.

Equation 1 is limited to the Porod term, although the complete description of the asymptotic SAXS intensity should to consider the asymptotic expansion of the intensity in case of sharp interfaces, i.e., the addition of three contributions: (1) the s^{-4} Porod term (K_P/s^4); (2) a series of oscillating terms associated with parallel interfaces (or parts of interfaces), whom origin has been first discussed by Ciccariello;[32] (3) the s^{-6} Kirste−Porod term (K_6/s^6) which has been first calculated by Kirste and Porod [33] in the case of smooth interfaces and later by Sobry et al.[34,35] in the case of angulous interfaces.

In the present study, no oscillations were observed on the tail-end of the SAXS curves and the oscillating terms were neglected. In contrast, it was shown[34] that the experimental SAXS intensity for the α,ω-metal sulfonato and carboxylato polyisoprenes was consistent with a significnt contribution of the s^{-6} term. K_6 is positive for smooth interfaces whereas the vertexes result in a negative contribution ($K_6 < 0$) in case of angulous interfaces.[34−36] The general vertex contribution to the s^{-6} term was calculated by Ciccariello and Sobry.[37] Very recently, Ciccariello and Sobry [38] have shown that the oscillations and the Kirste−Porod term are essentially independent of the existence of diffuse interfaces. This latter result is very important because the observation of a negative s^{-6} term is no longer related to the physical existence of a vertex. Indeed, provided that a phase is limited by three (or more) planes, the intersection of these planes result in a vertex contribution (s^{-6}) to the SAXS intensity. Therefore, the s^{-6} contribution observed in the SAXS intensity of the α,ω-metal sulfonato and carboxylato polyisoprenes must be related to the shape of the ionic aggregates.

K_6/K_P is the ratio of two successive terms of intensity and it does not depend on whether an absolute or a relative intensity is measured. Equation 3 is currently used for the analysis of two-phase systems, while eq 4 is the parent expression when the s^{-6} term has to be considered[35]

$$\frac{K_P}{Q} = \frac{S}{16\pi^5 V\varphi_1\varphi_2} \tag{3}$$

$$\frac{K_6}{K_P} = \frac{\Theta}{2\pi^2 S\varphi_1\varphi_2} \tag{4}$$

where $Q = 2\pi^2V\,(\Delta\rho)^2$ is the so-called invariant of Porod and $(\Delta\rho)^2$ is the mean-square electron density fluctuation. V is the

Table 1. Characteristic Θ_0, k_v, k_s, and ρ_0 Values for the Five Regular Polyhedra and for the Sphere

polyhedron	Θ_0	k_v[a]	k_s[a]	ρ_0
cube	−1.910	1.000	6.000	−113.09
tetrahedron	−5.285	0.118	1.732	−70.72
dodecahedron	−0.361	7.663	20.646	−8325.40
octahedron	0.626	0.471	3.464	298.82
icosaedron	2.337	2.182	8.660	58.39
sphere	6.283	4.189	12.566	18.62

[a] k_v and k_s are defined with respect to the edge length of the pohyhedron or to the radius r of the sphere.

sample volume and S is the total surface area of the interface. φ_1 and φ_2 are the volume fractions of phases 1 and 2. Θ is designated as the angulosity[34,35] or the sharpness[37] of the sample. Thus K_6/K_P is a measure of the angulosity per unit area of the scattering phases.

Θ is a pure number which only depends on the shape of the ionic aggregates. Let Θ_0 be the angulosity of a well-defined aggregate. The external surface S can be written as $k_s a^2$, where a is a characteristic length of this aggregate. Similarly, the volume is expressed as $k_v a^3$, where k_s and k_v are two geometrical constants. Very recently, Ciccariello and Sobry [37] have calculated the Θ contribution for the regular polyedra (cube, tetrahedron, octahedron, dodecahedron, icosahedron). Table 1 lists the values of Θ_0, k_v, and k_s for these polyedra.

Equations 3 and 4 can be combined into eq 5. The left-

$$\frac{k_s^3}{k_v^2\Theta_0} = 2\pi^2\left[\frac{K_P}{Q}\right]^2 \frac{K_P}{K_6} \tag{5}$$

handside of eq 5 is a constant for aggregates of a well-defined geometry and is designated as ρ_0 (Table 1)

$$\rho_0 = \frac{k_s^3}{k_v^2/\Theta_0} \tag{6}$$

ρ_0 is a pure number and is a generalization of the dimensionless S^3/V^2 ratio discussed by some of us in a previous paper.[34] The right-handside of eq 5, i.e., ρ_{exp}, directly results from the tail-end analysis of the SAXS curve. In the model ionomers, the polymeric phase (1) is dominant ($\varphi_1 \approx 1$) so that $V\varphi_1\varphi_2 - V\varphi_2 - V_2$ i.e., the volume of the ionic phase. Since S and V_2 are the external surface and volume of all the ionic aggregates, respectively, $S/(V\varphi_1\varphi_2) \approx S/V_2$ is the specific area of one ionic aggregate. Its value directly results from eq 3 while eqs 4 and 5 yield Θ/S and ρ_{exp}, respectively.

Taking into account the Kirste−Porod term, eq 1 can be written as follows, when s is large:

$$I \approx (K_P s^{-4} + K_6 s^{-6}) H^2(\sigma,s) \tag{7}$$

If σs were small, eq 8 would be an acceptable approximation

$$I \approx (K_P s^{-4} + K_6 s^{-6})(1 - 4\pi^2\sigma^2 s^2) \tag{8}$$

The Is^4 vs s^2 plot is commonly used to determine σ from the slope of the short "straight line portion". Figure 1 shows that the slope decreases when the broadening function is L, V, G, and R, respectively. Therefore, for a given experimental slope, the calculated σ values compare as follows: $\sigma_R \geq \sigma_G \geq \sigma_V \geq \sigma_L$. The four functions however yield the same σ value when σs is very small. Since the asymptotic Porod law is only valid at large s values, a unique value of σ is only obtained when σ is extremely small. According to Koberstein et al.,[28] the Mac Laurin approximation (eq 8) may be used in the first part of the decreasing tail end of the curve only if σs is small enough. To improve the accuracy of the information extracted from the tail end of the SAXS curve, the data treatment has been revised in this paper.

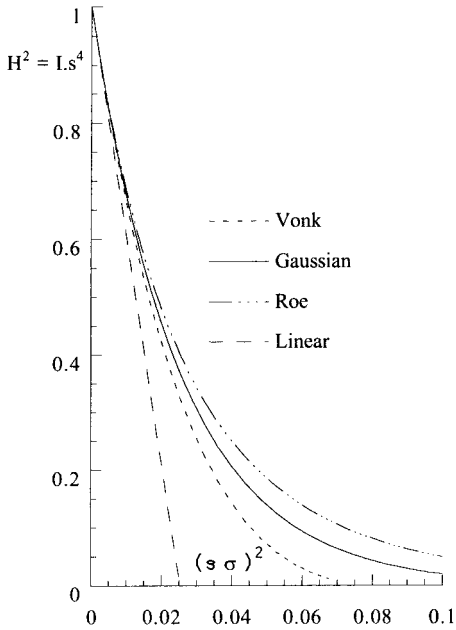

Figure 1. Plot of normalized $H^2(\sigma s)$ vs $(\sigma s)^2$ for the Gaussian, Vonk, and Roe functions and their linear approximation.

The major problem results from the need to smear eq 1 (or eq 7) for it to be applicable to smeared experimental data. In this respect, Kobertsein et al.[28] have suggested various approximations in case of sigmoidal profile and infinite slit length. When this approximation is not valid, the smearing of the s^{-4} term does not result in a s^{-3} term. Todo et al.[39] have shown that the smearing of a s^{-4} term leads to an $s^{-\alpha}$ term, whereas a s^{-2} term yields a $s^{-\beta}$ term. The correct value of α and β depends on both the s range and the effective slit length profile used in the SAXS experiment. Similarily, $s^{-\gamma}$ is the smeared term corresponding to a s^{-6} term. In this study, typical values for α, β, and γ are as follows: $\alpha = 3.25$, $\beta = 1.50$, and $\gamma = 5.15$ with a standard deviation of 0.02. They have been calculated by the method developed by Baldrian and Soler[40] and on the assumption that the experimental slit length profile is a succession of linear segments. The calculated smeared intensities, $\tilde{I}(s)$, corresponding to the various powers of s, have been fitted by linear least-squares analysis so as to determine α, β, and γ.

From eq 8, the smeared intensity $\tilde{I}$ may be written as follows:

$$\tilde{I} \approx \tilde{K}_P s^{-\alpha} - \tilde{K}'_P s^{-\beta} + \tilde{K}_6 s^{-\gamma} \tag{9}$$

or

$$S^\alpha \tilde{I} \approx s^\alpha \tilde{K}_P - \tilde{K}'_P s^{\alpha-\beta} + \tilde{K}_6 s^{\alpha-\gamma} \tag{10}$$

where $\tilde{K}_P$, $\tilde{K}'_P$ and $\tilde{K}_6$ are the smeared coefficients of the s^{-4}, s^{-2}, and s^{-6} terms, respectively. $s^{\alpha-\gamma}$ is always decreasing ($\gamma > \alpha$). $\tilde{K}_6$ is positive for smooth interfaces[34] so that the additional term $K_6 s^{\alpha-\gamma}$ in eq 10 is decreasing when s is increased. However, in case of angulous interfaces, $\tilde{K}_6$ is negative and $\tilde{I}s^\alpha$ first increases with s, before decreasing when the $s^{\alpha-\beta}$ term becomes dominant. Figure 2 is a typical example of the $\tilde{I}s^\alpha$ vs s^α plots observed in this study, which clearly shows a maximum in the Porod region. This maximum results from a negative $\tilde{K}_6$ contribution and thus from angulous interfaces as mentioned before.

The linear least-squares analysis of the smeared intensity with eq 9 provides a good fit, and the extracted $\tilde{K}_P$, $\tilde{K}'_P$, and $\tilde{K}_6$ values have proved to be suitable for the subsequent refinement by using eq 7, which includes the analytical broadening function $H^2(\sigma,s)$. Equation 7, which is smeared by numerical integration for all the observed positions of the smeared intensity and the least-squares refinement, aims at

Figure 2. Plot of Is^{α} ($\alpha = 3.25$) vs s^{α} for PIP−S−Sr-8000. The maximum at 0.14 in the Porod region ($s = 0.55$ nm^{-1}) is the signature of a angulous contribution to the tail-end of the scattering curve.

minimizing the sum of squares of the differences between $\tilde{I}_{exp}$ and $\tilde{I}_{calc}$. Corrections are repeated until they are smaller than 1% for each parameter, which usually requires three or four refinement cycles. It is worth noting that during the refinement process, the K_6/K_P ratio remains essentially constant while the individual parameters tend to their final value. This ratio is thus an intrinsic property of the tail end of the SAXS curve.

Results

The polyisoprene (PIP) samples that have been studied are listed in Table 2 and identified with respect to the anion (S for sulfonates, PIP−S; and C for carboxylates, PIP−C), the metal cation (Na, K, Rb, Cs, Mg, Ca, Sr, and Ba) and the molecular weight (M_n). Moreover, an α,ω-carboxylic acid polyisoprene ($M_n = 8500$) has been neutralized at various extents (from 75 to 150%) with potassium methoxide.

The so-called "ionic peak" is clearly observed for each sample as reported in Figure 3a in the case of α,ω-potassium sulfonato polyisoprenes. Similar figures are deposited for cases α,ω-barium sulfonato polyisoprenes and α,ω-barium carboxylato polyisoprenes. It is however missing for the unneutralized diacid precursor. The position of the ionic peak, s_{IP}, is reported with respect to the baseline in order to be free from overlapping and shift effects. Indeed the ionic peak is superimposed to the decreasing SAXS scattering curve that results from organization at distances much larger than $d_{IP} = 1/s_{IP}$. The overlapping of the baseline and the ionic peak results in a shift of the maximum intensity position toward smaller angles. The spacing Bragg distances, d_{IP}, as calculated from s_{IP}, are listed in Table 2, together with the distance d_2 for a second peak, usually observed at larger angles. For the sake of comparison, the root-mean-square end-to-end distance, r_{rms}, has been calculated for the polyisoprene precursor in the unperturbed state.[41]

Table 2 also reports the main data extracted from the analysis of the tail-end of the experimental curves, i.e., the interphase width $E = 12^{1/2}\sigma$, the specific area of the ionic aggregates S/V_2, the angulosity per unit area Θ/S, and the right-hand side member of eq 13, i.e., ρ_{exp}. These parameters have been calculated for the three previously discussed interphase profiles (*G*, *V*, and *R*) and the linear approximation (*L*) as well. Since the results are quite similar, they are only reported for the Gaussian profile. This aspect will be discussed in a next section.

For the purpose of comparison, the SAXS curves have been scaled in such a way that the ionic peak position and the maximum in intensity are the same for all the samples. They are reported in figures 3b and 4a,b.

Effect of the Polyisoprene Molecular Weight. Figure 3a shows that the ionic peak position moves toward smaller angles and thus that the associated Bragg distance d_{IP} increases upon increasing molecular weight.

A log−log plot of the Bragg distance vs the molecular weight for the three studied series of samples shows a power law of the $d_{IP} = k(M_n)^n$ form, where *k* and *n* are two constants to be determined by linear regression. The *n* exponent is close to 0.5 for the two series of sulfonato-telechelic polyisoprenes (0.50 for S−K and 0.48 for S−Ba) which means that it is essentially independent of the metal cation at least when alkali-metal and alkaline-earth-metal cations are concerned. Only three samples of the carboxylate series are available, which makes the *n* value uncertain. Keeping this limitation in mind, the experimental data are also consistent with $n = 0.5$. The following equations have accordingly been derived from Figure 5:

$$\text{PIP−S−K(Ba)} \quad d_{IP} = 0.074(M_n)^{0.5} \tag{11}$$

$$\text{PIP−C−Ba} \quad d_{IP} = 0.053(M_n)^{0.5} \tag{12}$$

It is worth noting that the ratio of the two proportionality constants is nearly equal to $2^{1/2}$. Furthermore, Table 2 shows that d_{IP} is approximately equal to the mean square end-to-end distance, r_{rms}, for the PIP−S samples and to $r_{rms}/2^{1/2}$ for the PIP−C samples whatever the molecular weight and the metal cation.

The intraparticle interference model does not provide an acceptable explanation for these observations, in contrast to the interparticle interference. Indeed, d_{IP} is related to a repeative distance between reticular planes of the ionic aggregates organization and thus d_{IP} is proportional to the distance between the ionic nodules, d_{IN}. Due to the selective localization of the ionic groups at both ends of linear PIP chains, the internodular distance, d_{IN}, is expected to change with the chain molecular weight as r_{rms} does, in agreement with experiments.

If the basic linear relationships between M_n and $(r_{rms})^2$ for unperturbated chains is extended to the Bragg distance, it results from eqs 11 and 12 that d_{IP} must be proportional to r_{rms}. This is confirmed by the ratio d_{IP}/r_{rms}, which is constant for the investigated samples whatever the molecular weight and the cation. Dependence of d_{IP} and r_{rms} is reported in Figure 6, in agreement with

$$d_{IP} = 0.95 r_{rms} \quad \text{for the PIP−S series} \tag{13}$$

$$d_{IP} = 0.68 r_{rms} \quad \text{for the PIP−C series} \tag{14}$$

with a correlation coefficient of 0.978 in both cases.

Table 2. Experimental SAXS Data for the Investigated Telechelic Polyisoprenes

samples											
anion	cation	$10^{-3}M_n$	d_{IP} (nm)	r_{rms} (nm)	d_{IP}/r_{rms}	d_2 (nm)	d_{IP}/d_2	E (nm)	S/V_2 (nm^{-1})	θ/S (nm^{-2})	ρ_{exp}
S	K	5.5	5.60	5.76	0.97	3.41	1.64	0.24	14.4	−2.97	−69.4
S	Ba	5.5	5.86	5.76	1.02	3.55	1.65	*1.58*	*23.7*	*	*
S	Na	8	6.48	6.95	0.93			0.20	17.7	−3.19	−98.1
S	K	8	6.37	6.95	0.92			0.11	15.4	−3.13	−75.2
S	Rb	8	6.43	6.95	0.93			0.20	14.9	−3.09	−72.0
S	Cs	8	6.34	6.95	0.91	3.57	1.78	0.08	15.1	−3.05	−75.2
S	Mg	8	5.97	6.95	0.86	3.19	1.87	*0.94*	*37.1*	*−2.99*	*−459.3*
S	Ca	8	5.96	6.95	0.86	3.08	1.94	0.32	22.3	−3.42	−145.3
S	Sr	8	6.07	6.95	0.87	3.33	1.82	0.46	20.5	−3.02	−138.8
S	Ba	8	6.12	6.95	0.88	3.53	1.73	0.22	18.0	−3.08	−98.8
S	K	14.5	9.17	9.40	0.98	5.49	1.67	0.24	21.3	−3.32	−136.3
S	Ba	14.5	9.18	9.40	0.98	5.39	1.70	0.22	19.2	−3.28	−112.5
S	K	16	8.93	9.80	0.91	5.60	1.59	0.26	21.0	−3.47	−127.6
S	Ba	16	8.92	9.80	0.91	5.36	1.66	*0.58*	*21.6*	*−2.88*	*−161.2*
S	K	21	10.93	11.30	0.97			0.29	23.3	−3.46	−156.3
S	Ba	21	10.62	11.30	0.94	6.42	1.65	0.19	18.6	−3.15	−109.6
C	Ba	5	4.05	5.50	0.74	2.27	1.78	0.30	21.9	−3.23	−148.4
C-0.75	K	8.5	4.92	7.20	0.68			0.29	18.7	−2.99	−116.7
C-0.95	K	8.5	5.03	7.20	0.70	2.88	1.75	0.40	17.1	−3.02	−96.5
C-1.05	K	8.5	5.08	7.20	0.71	2.91	1.75	*0.55*	*19.7*	*−2.57*	*−150.3*
C-1.20	K	8.5	5.12	7.20	0.71			0.36	19.2	−2.99	−113.4
C-1.50	K	8.5	5.38	7.20	0.75	2.98	1.81	0.20	17.0	−3.02	−95.4
C	Ca	8.5	4.79	7.20	0.67	2.63	1.82	*0.83*	*38.2*	*−2.93*	*−497.8*
C	Ba	8.5	4.76	7.20	0.66	2.68	1.78	0.15	18.3	−3.03	−110.8
C	Ba	15	6.15	9.50	0.65	3.70	1.66	0.28	20.2	−3.06	−133.1

From parts a and b of Figure 4, the shape of the ionic peak markedly depends on the nature of the anion. In the PIP−S−Ba case, the ionic peak intensity is significantly more intense and its width at half-height, δ, is smaller compared to the PIP−C−Ba analogue. When α,ω-sulfonic acid polyisoprenes are neutralized with potassium (Figure 3b) rather than with barium (Figure 4a), the ionic peak intensity decreases while δ remains unchanged. Moreover, the ionic peak intensity of the sulfonate series regularly decreases as the chain length is increased, and for the highest M_n (21 000), the ionic peak only appears as a shoulder on the scattering curve. In contrast, the samples with carboxylate end groups do not exhibit this regular decrease in intensity upon increasing M_n. These observations can be accounted for by the decrease in the volume fraction of the ionic phase when M_n is increased and by the lower electronic contrast of potassium compared to Ba and of carboxylates compared to sulfonates, respectively. Furthermore, the decrease in the ionic peak intensity results in a shift of the foot of the strong upturn of the SAXS curve toward smaller angles.

In all the cases, the ionic peak is asymmetric, which results from the reciprocal relationship between s/s_{IP} and d/d_{IP} ($s = 1/d$). Indeed, a plot of I vs d restores the symmetry of the ionic peak. Thus, the asymmetry of the ionic peak results from a symmetrical distribution of the internodular distances with respect to a mean distance, d_{IN}. The dispersion increases with M_n and is larger in the PIP−S series than in the PIP−C series.

The Observation of a SAXS Side Maximum. Most investigated samples (Figures 3b and 4a,b) show a shoulder or a very weak maximum on the right-hand side of the ionic peak at a d_{IP}/d_2 position in the range 1.60−1.85, that reflects the poor accuracy of this additional SAXS contribution. The d_2/d_{IP} ratios are listed in Table 2. Such an observation has already been reported for halato-telechelic polybutadienes and interpreted as an indication for a lamellar morphology ($d_2 = 2d_{IP}$[5,6,23]). In this study, the average ratio is close to $3^{1/2}$, which is consistent with a hexagonal organization of the ionic aggregates.

To confirm this hypothesis two new samples, PIP−S−K ($M_n = 5000$) and PIP−C−K ($M_n = 11200$), have been analyzed by SAXS with entrance slits of 40 and 125 μm, respectively, and with such a high number of steps that 450 experimental data have been collected over the whole curve. The ionic peak positions, i.e., 5.29 nm for the PIP−S−K 5 and 5.49 nm for the PIP−C−K 11.2, agree with the values predicted from the two previous equations, 11 and 12. Although very weak, satellite peaks are observed as shown by the pinhole curves (Figure 7a). The relative position of the satellite peaks with respect to the ionic peak are listed in Table 3 and compared to the theoretical values for a hexagonal array. The agreement is satisfactory and definitely better that for a cubic or a quadratic model. The dispersion of the internodular distance with respect to the average value, d_{IN}, makes the satellite peaks apparently less intense or completely unobserved. It is known that noise in the smeared data can get accentuated during desmearing. However, these satellites peaks are observed, at the same positions, whatever the desmearing procedure used.[26,27] It has also been verified that the origin of the peak in the pinhole curve corresponds to a bump and not to noise in the experimental smeared curve. The systematic observation of such peaks at similar positions in most investigated samples confirms the reality of these small peaks.

Ionic Peak Position and Internodular Distance. From the aforementioned data, it might be proposed that the ionic aggregates organize themselves according to a planar hexagonal array with a characteristic distance d_{IN}. The first observed interplanar distance, d_{IP}, is equal to $(3^{1/2}/2)d_{IN}$ and the distance between two ionic nodules, d_{IN}, would approximately be 1.15-d_{IP}, so that eqs 13 and 14 yield eqs 15 and 16 for d_{IN}. Equations 15 and 16 indicate that the planar

$$d_{IN} = 1.09r_{rms} \quad \text{for the PIP−S series} \qquad (15)$$

$$d_{IN} = 0.78r_{rms} \quad \text{for the PIP−C series} \qquad (16)$$

hexagonal array of the ionic aggregates keeps the PIP

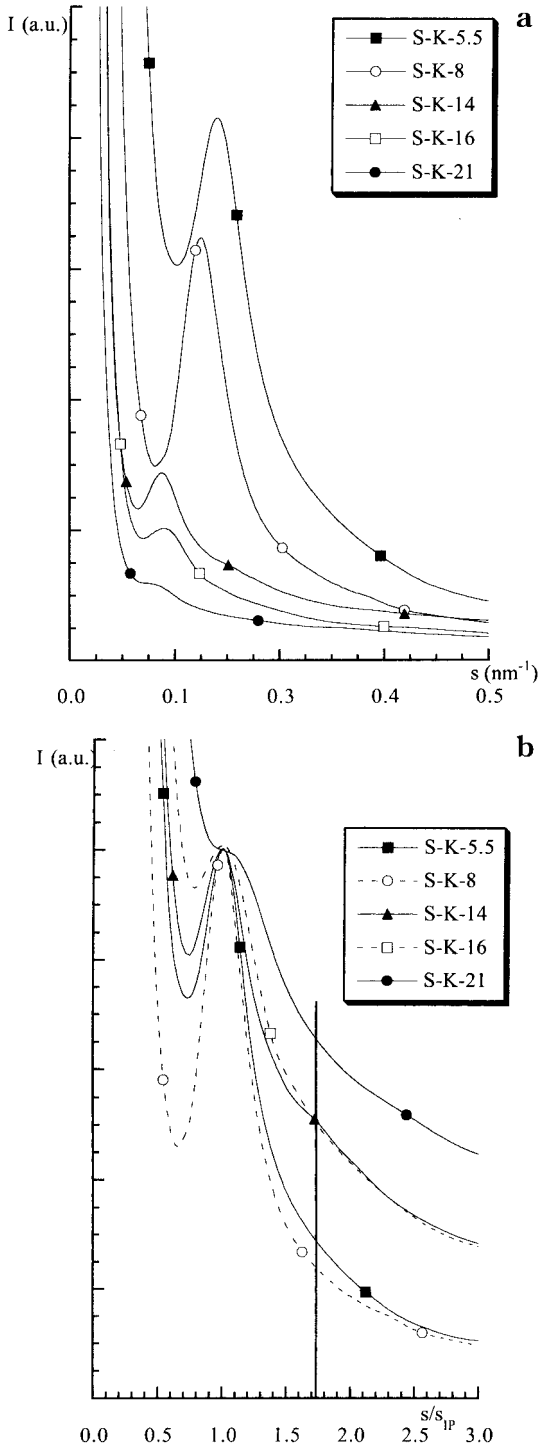

Figure 3. (a) Pinhole intensity (in arbitrary units) vs s (nm^{-1}) for α,ω-potassium sulfonato polyisoprenes. The SAXS curves have been shifted upward for the sake of clarity. (b) Normalized pinhole intensity in arbitrary units vs s/s_{IP} for the same samples. The intensity is normalized to 1 at the ionic peak position ($s/s_{IP} = 1$). The vertical line indicates the expected position for the first satellite peak ($s/s_{IP} = 1.73$).

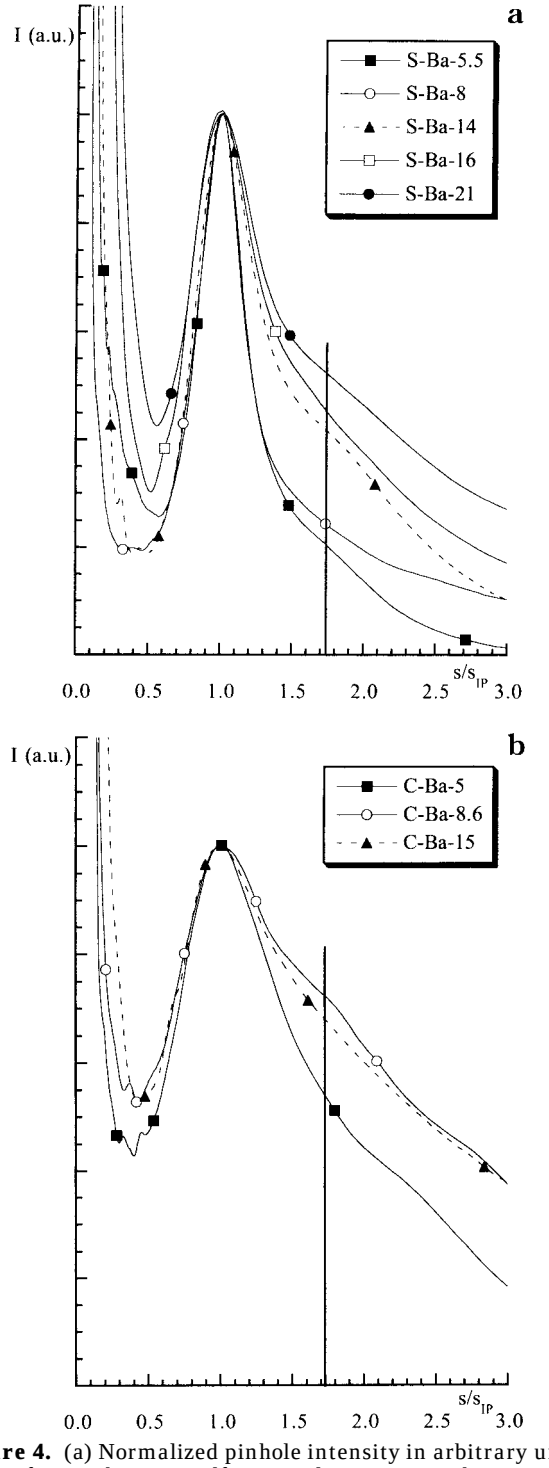

Figure 4. (a) Normalized pinhole intensity in arbitrary units vs s/s_{IP} for α,ω-barium sulfonato polyisoprenes. The intensity is normalized to 1 at the ionic peak position ($s/s_{IP} = 1$). The vertical line indicates the expected position for the first satellite peak ($s/s_{IP} = 1.73$). (b) Normalized pinhole intensity in arbitrary units vs s/s_{IP} for α,ω-Ba carboxylato polyisoprenes. The intensity is normalized to 1 at the ionic peak position ($s/s_{IP} = 1$). The vertical line indicates the expected position for the first satellite peak ($s/s_{IP} = 1.73$).

chains essentially unperturbed when the end-groups are metal sulfonates. In contrast, the same spatial organization of the ionic aggregates requires some chain contraction with respect to the unperturbed conformation when metal carboxylates are substituted for the metal sulfonate end groups, all other conditions being the same.

According to the Eisenberg, Hurd, and Moore model of ionomer morphology,[3] an extension of the polymer chain segments located in the vicinity of the multiplets is expected. This extension is believed to be more pronouced for metal sulfonate end-groups.

Influence of the Cation Nature. Table 2 reports the Bragg's spacing for the α,ω-sulfonic acid PIP of a 8000 molecular weight polymer, which was neutralized with various alkal-metal and alkaline earth-metal cations.

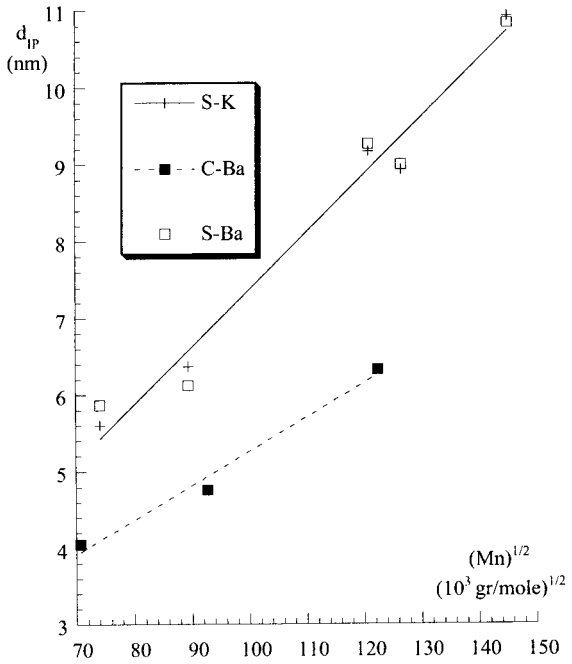

Figure 5. Plot of d_{IP} vs $M_n^{0.5}$ for sulfonato- and carboxylato-telechelic PIP.

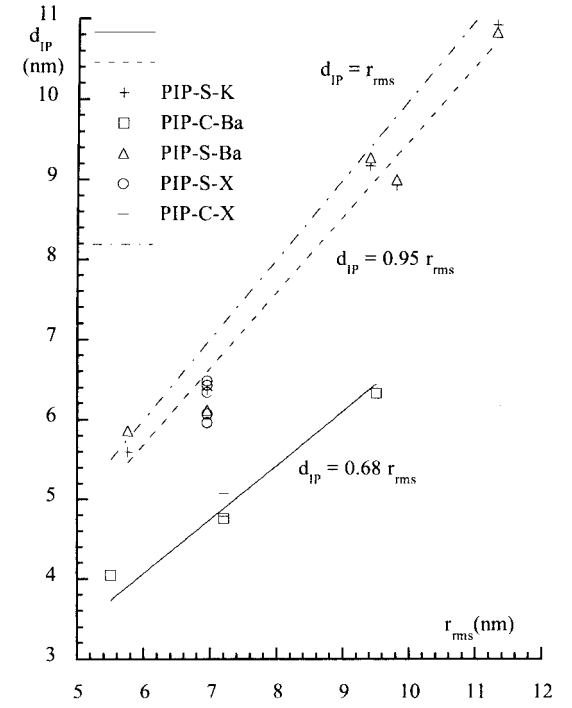

Figure 6. Plot of d_{IP} vs r_{rms} for sulfonato- and carboxylato-telechelic PIP.

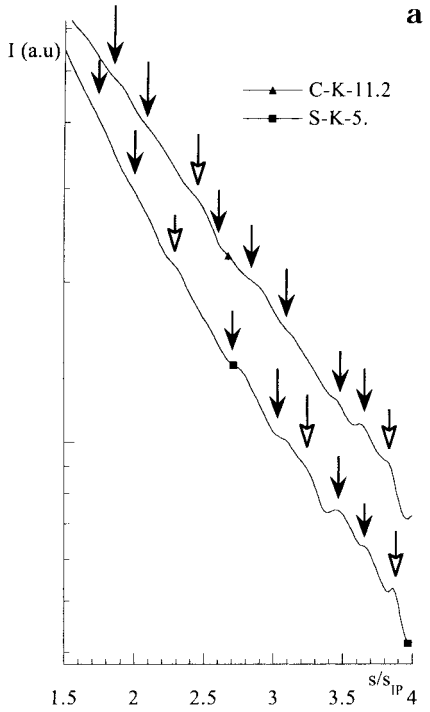

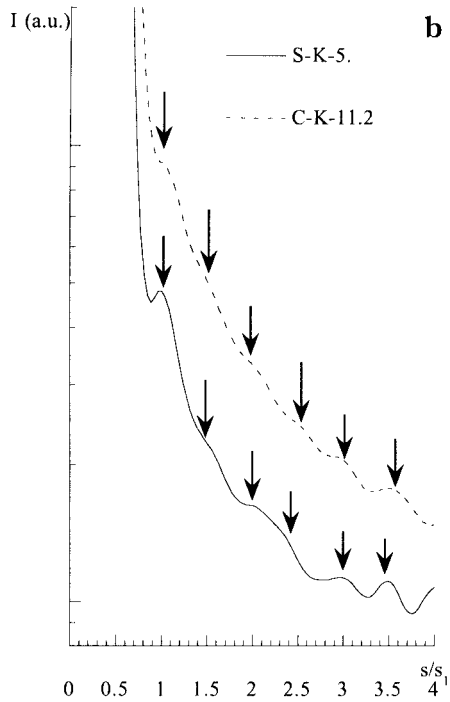

Figure 7. (a) Plot of the pinhole Porod intensity vs s/s_{IP} for the two extra samples C−K 11.2 and S−K 5.0. The arrows indicate the satellite peak positions reported in Table 3. Black arrows indicate hexagonal peaks while white arrows marks supplementary peaks. (b) Plot of the pinhole Porod intensity vs s/s_1 for the two extra samples C−K 11.2 and S−K 5.0. s_1 is the s position of the first peak of the superstructure. The arrows indicate the supplementary peak positions reported in Table 3.

In contrast to the anion, the countercation has little influence upon the characteristic periodicity and the shape and intensity of the ionic peak. It is however surprising that the highest intensity in the alkali-metal series is observed for sodium (Figure 8). This observation might be explained by the smaller radius, r, of Na (0.98 Å) compared to K (1.33 Å), Rb (1.48 Å) and Cs (1.67 Å), so that the electronic contrast between the ionic aggregate and the polymeric matrix, $Z/r^3 - \eta$, is larger when Na is concerned, η being the electronic density of the polymer matrix; in any case, η is smaller than Z/r^3. The same discussion holds for the alkaline-earth-metal series in which the highest intensity is observed for Ba and the lowest for Ca.

Clearly, the cation has no significant influence on the chain conformation and the distribution of the ionic aggregates within the polymeric matrix. Therefore, d_{IN}, being the average distance between the gravity center of two near-neighbor nodules, the difference of 3−4 Å

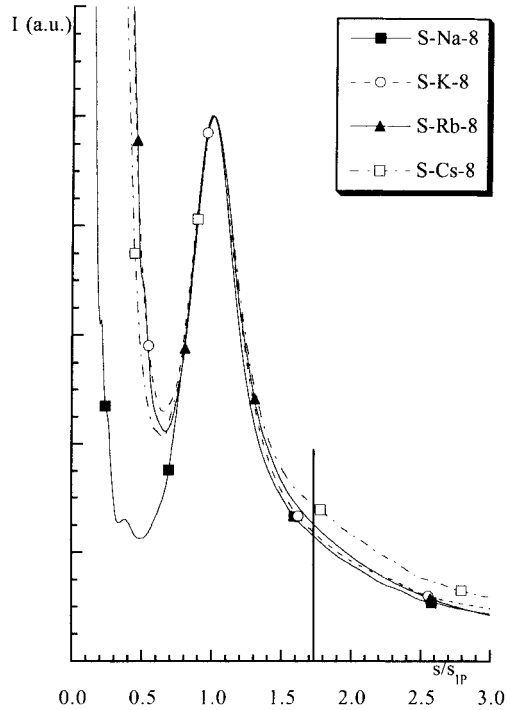

Figure 8. Normalized pinhole intensity in arbitrary units vs s/s_{IP} for for α,ω-X sulfonato polyisoprenes (M_n = 8000; X = Na, K, Rb, Cs). The intesity is normalized to 1 at the ionic peak position (s/s_{IP} = 1). The vertical line indicates the expected position for the first satellite peak (s/s_{IP} = 1.73).

Table 3. Relative Position (s/s_{IP}) of the Successive Satellite Peaks, Experimental Bragg Spacings and Ratios (s/s_1) of the Peaks with Respect to the First Peak at Very Small Angles and Theoretical Relative Positions of Satellite Peaks with Respect to the First Peak in the Case of a Hexagonal Array

PIP-C-K-11.2			PIP-S-K-5.0			theoretical
s/s_{IP}	d (nm)	s/s_1	s/s_{IP}	d (nm)	s/s_1	ratio
	116.	1.00		131.	1.00	1.00
1.84	75.	1.54	1.73	85.	1.54	1.73
2.06	57.	2.02	2.01	63.	2.04	2.00
2.49			2.33			
2.89	45.7	2.54	2.73	53.	2.46	2.65
3.08	38.0	3.05	3.01	43.2	3.03	3.00
3.47	32.5	3.57	3.51	37.1	3.53	3.46
3.68			3.68			3.61
3.85			3.87			4.00

in d_{IN} between the series of alkali-metal and alkaline-earth-metal cations has something to do with a change in the nodule size. Indeed, for a constant number of sulfonic groups per ionic nodule, the size of the nodule is expected to increase while going from alkaline-earth-metal cations to twice as many alkal ones.

Influence of the Degree of Neutralization. Table 2 and Figure 9 show how the Bragg periodicity changes with the degree of neutralization of the α,ω-carboxylic acid polyisoprene.

At a neutralization degree of 75%, the ionic peak is visible, which indicates that the material is microphase-separated. Upon increasing neutralization, an acid proton is merely replaced by a metal ion, which accounts for the apparent constancy of d_{IN} as it can be seen from Figure 9. In contrast, an excess of neutralization agent is responsible for a slight increase in the Bragg spacing, i.e., in the size of the ionic domains. This increase is on the same order of magnitude as the difference observed between the family of the alkaline-earth-metal ions and the family of the alkali-metal ions which require twice as many metallic ions for a 100% neutralization. It is also observed that the ionic peak intensity is the highest when the neutralization is complete, which may be a clue for a better organization of the ionic aggregates. When the neutralization degree is lower or much larger than 100%, the structure of the microdomains is perturbed as shown by a decreasing intensity of the ionic peak and an increasing dispersion of the internodular distance (Figure 9). Furthermore, the position of the origin of the intensity upturn at very small s is observed at increasing s values as the neutralization degree is increased. This observation is consistent with the explanation according to which isolated ions dispersed within the polymeric matrix are responsible for the intensity upturn.[17−23]

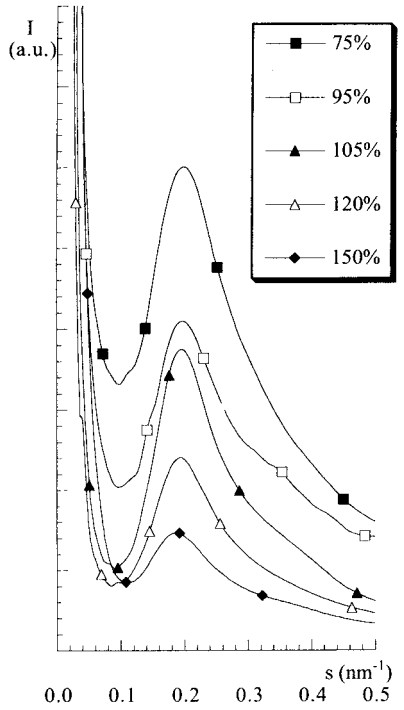

Figure 9. Pinhole intensity (in arbitrary units) vs s (nm^{-1}) for α,ω-potassium carboxylate polyisoprenes neutralized at various extents. The SAXS curves have been shifted upward for the sake of clarity.

A Possible Superstructure of the Ionic Microdomains. The sharp increase in intensity, which is observed at very low angles.[2,3,6] prevents the radius of gyration of the scattering particles from being estimated by the Guinier law.[7] No linearity in the plot of ln[$I(s)$] vs s^2 has been observed, even though the intensity has been measured at s as small as 0.013 nm^{-1} (i.e., $2\theta = 10^{-3}$ rad).

It is worth recalling that a series of peaks characteristic of a hexagonal organization are superimposed on the SAXS curve at very low angles in the case of barium, magnesium, and sodium carboxylato-telechelic poly(*tert*-butyl acrylate)s (PtBA) (M_n = 21 000).[42] The Bragg spacings then range from 70 to 14 nm. This observation has been confirmed for various molecular weights (from 5000 and 64000) under various experimental conditions.[43] Since the SAXS curves of the halato-telechelic polyisoprenes show clear maxima in the vicinity of s = 0.05 nm^{-1}, the analysis of two samples (M_n = 5000 and M_n = 11200) have been repeated by collecting a great number of data at very low angles. The pinhole curves,

Table 4. Effect of the Polymer Backbone on the Ionic Peak Position

polymer	$10^{-3}M_n$	d_{IP} (nm)	r_{rms} (nm)	d_{IP}/r_{rms}
PSt-C-Ba	5.3	3.70	5.0	0.74
PIP-C-Ba	5.0	4.05	5.5	0.74
PBD-C-Ba	4.6	7.00	7.0	1.00

shown in Figure 7b, do not depend on the desmearing procedure. They have been plotted vs normalized s/s_1 values, where s_1 is the position of the first maximum position. Similarly to the previously studied poly(*tert*-butyl acrylate) samples, a series of clearly defined peaks are unambiguously observed in a possible relation to a supraorganization. The Bragg spacings range from 120 to 20 nm. The ratios of the successive Bragg spacings with respect to the first one (s_1) are in good agreement with the theoretical values for a hexagonal structure (Table 3). Comparison of data collected for PtBA and PIP indicates larger distances for PIP compared to PtBA. Although not determined for PtBA,[42] the characteristic dimension of the hexagonal suprastructure is on the order of $20-30d_{IP}$ for PIP-containing samples. In particular, it is observed that the characteristic dimension is slightly greater for the PIP−S−K-5.0 sample (131 nm) than for PIP−C−K-11.2 sample (116 nm). This observation agrees with the systematic observation of smaller d_{IP} in the carboxylates when compared to d_{IP} values for sulfonates of same molecular weight. The corresponding d_{IP} values are respectively 5.29 and 5.49 nm for the sulfonate and the carboxylate sample, respectively. However, the difference between the characteristic dimensions is very small, and moreover the first peak position (Figure 7b) in the carboxylate sample is less precise than in the sulfonate one. The hypertstructure characteristic dimension follows the double trends of increasing with increasing molecular weight and decreasing when sulfonates are replaced by carboxylates.

Influence of the Prepolymer Backbone. Table 4 compares the Bragg spacings for carboxylatotelechelic polystyrene, polyisoprene and polybutadiene[7] of comparable M_n.

Carboxylato-telechelic polystyrene and polyisoprene show a chain contraction with respect to the unperturbed dimension, in contrast to the polybutadiene analogue for which the d_{IP}/r_{rms} ratio is 1. The reason for this surprising observation might be found in the experimental conditions used for the synthesis of these telechelic polymers. Actually, polystyrene and polyisoprene telechelics have been synthesized by living anionic polymerization and deactivation of the living chains by CO_2. These polymers are of a narrow molecular weight distribution (MWD), in contrast to the polybutadiene sample that has been synthesized by a radical process with a carboxylic acid containing a symmetric azo compound as an initiator. The large difference in MWD (1.8 compared to 1.15) must have an effect on the related tridimensionnal network, which might explain the differences reported in Table 4.

Analysis of the Tail End of the Curve. Values of E, S/V_2 and Θ/S (Table 2) results from the analysis of the tail end of the SAXS curves with a Gaussian $H^2(\sigma,s)$ function. Values of the S−Mg-8, S−Ba-5.5, S−Ba-16, C−K-8.6 (105%) and C−Ca-8.6 samples are questionable and reported in italics in Table 2. Indeed, the number of experimental data for these samples is not large enough for the background subtraction and the tail end analysis to be accurate. In fact, these samples were registered at the beginning of this study and rapidly, it appears that the number of experimental points necessary for a correct tail end analysis must be increased. At tis time, it was not possible to again register the SAXS curve of these five samples. The least-squares analysis provide error estimates for the parameters which are directly determined (B_0, B_2, K_P, K_6, and σ). They are systematically of the order of a few percents (1 to 3 depending on the sample). It is quite reasonnable to consider that the errors on S/V_2 and on Θ/S are on the order of 2−5%s. The maximum error on ρ_{exp} is thus on the order of 6−15%s.

Comparison between of the four functions (L, G, V, R) shows a good agreement for the Θ/S values, except for the L function of C−Ca-8.6. This is not surprising since the s^{-6} term mainly affects the first part of the Porod region and allows the four functions to be approximated by the same Mac Laurin development.

The specific area S/V_2 is 10 to 20% larger when the Roe function is used rather than the Gaussian function. The linear approximation yields lower S/V_2 values and the discrepancy increases with S/V_2 (Figure 10). A least-squares fitting agrees with eq 17, with a correlation coefficient of 0.993 and nm^{-1} units.

$$(S/V_2)_R = -1.34 + 1.20(S/V_2)_G \qquad (17)$$

In case of the Vonk function, the difference with respect to the Gaussian can reach 20%, S/V_2 being greater or smaller than the related Gaussian value.

The interphase thickness, E, depends on the function used for the calculation, which clearly appears when $\Delta E_X/E_G$ is plotted vs E_G, where $\Delta E_X = E_X - E_G$ and X stands for R, V, and L. The equations for the linear dependence of $\Delta E_X/E_G$ on E_G are reported in Figure 11. It is a good approximation to consider that ΔE_X is proportional to the square of E_G (eq 18). Clearly, L is

$$\Delta E_R = 0.19(E_G)^2 \quad E_V = -0.14(E_G)^2$$
$$\Delta E_L = -0.38(E_G)^2 \qquad (18)$$

the worst approximation, whereas V yields a smaller interphase thickness than G and R gives a wider interphase.

From thermodynamic considerations, the R function more likely yields the best solution. Complexity of the related developments explains why the Gaussian values have been considered.

Except for the five samples, the analysis of which is questionable, $(S/V_2)_G$ is essentially constant (14.4−22.3 nm^{-1}) and E_G varies from 0.11 to 0.46 nm without any apparent dependence on the structural parameters of the investigated samples. S/V_2 is the specific area of the ionic aggregates from which a characteristic distance can be calculated, e.g. $6/D$ and $6/a$ for spherical aggregates of a diameter D and cubic aggregates of an edge a, respectively. In this study, this characteristic distance can be approximated to 3.3 Å. The PIP−S samples of $M_n = 8000$ show that S/V_2 decreases when the ionic radius increases (Na, K, Rb, and Cs for monovalent cations and Mg, Ca, Sr, and Ba for bivalent cations) in agreement with an increase in V_2 as the ionic radius of the constitutive cations is increased. Two structural models can be proposed. Either the anionic groups (carboxylates or sulfonates) form the interphase between the polyisoprene matrix and the cations, or the anions and cations are integral parts of the ionic phase

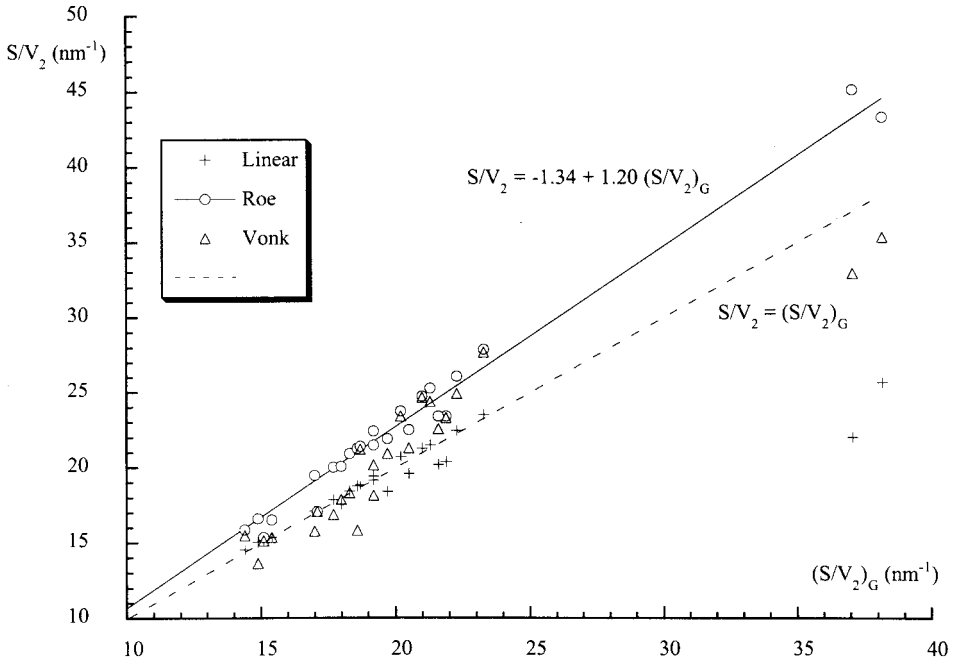

Figure 10. Plot of S/V_2 vs $(S/V_2)_G$ for the three *R*, *V*, and *L* functions.

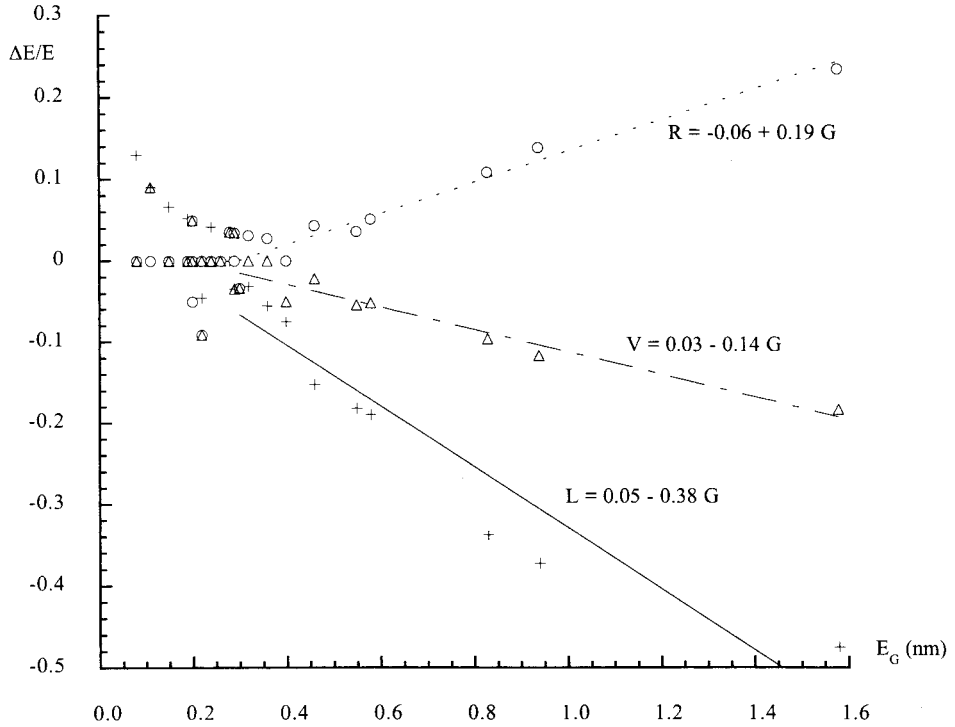

Figure 11. Plot of $\Delta E/E$ vs E_G for the three *R*, *V*, and *L* functions.

and the interphase then results from some diffuse mixing of the chain segments and the ionic groups. Only the first proposal, referred to as the "cationic model", accounts for the highest intensity of PIP−S−Na in the series of the alkaline sulfonates. It is also consistent with S/V_2 that increases with the cation radius.

The angulosity, Θ/S, is in the range −2.97 to −3.47 nm^{-2}. On the assumption that all the ionic aggregates are of the same shape in all the polyisoprenes samples, Θ is constant and Θ/S is dictated by the *S* value. According to Table 2, Θ/S decreases when the cation radius increases, which agrees with the "cationic model". Furthermore, at constant M_n, Θ/S is smaller for PIP−S−Ba compared to PIP−S−K. The ionic radius is the same for both cations, and the difference in Θ/S has to be found in the number of cations per ionic aggregate. Indeed, the number of monovalent cations must be twice the number of divalent cations for a constant number of chains per ionic aggregate. Finally, Θ/S increases with the PIP molecular weight in the PIP−S−K series. Indeed, in the second proposal, the SAXS intensity of the ionic peak does slightly depend on the nature of the cation and it will be the smallest for Na and Mg counterions, having the smallest electronic density.

The Shape of the Ionic Aggregates. Comparison of the ρ_{exp} values (from −69,35 and −145,28 in Table 2) with theoretical ρ_0 (Table 1) gives credit to cubic

Table 5. Tail End Analysis of the SAXS Data for the Tetrahedric Aggregation Model and the Equilateral Prismatic Model

samples				tetrahedron				equilateral prism			
anion	cation	$10^{-3}M_n$	ρ_{exp}	S (nm^2)	a_s (nm)	V_2 (nm^3)	a_s/a_v	S_{prism} (nm^2)	a_s (nm)	V_2 (nm^3)	a_s/a_v
S	K	5.5	−69.4	1.78	1.01	0.124	1.00	1.06	0.80	0.074	0.93
S	Na	8	−98.1	1.66	0.98	0.094	1.06	0.99	0.77	0.056	0.98
S	K	8	−75.2	1.69	0.99	0.110	1.01	1.01	0.78	0.066	0.94
S	Rb	8	−72.0	1.71	0.99	0.115	1.00	1.02	0.78	0.069	0.93
S	Cs	8	−75.2	1.73	1.00	0.114	1.01	1.04	0.79	0.068	0.94
S	Ca	8	−145.3	1.55	0.95	0.069	1.13	0.92	0.74	0.042	1.05
S	Sr	8	−138.8	1.75	1.00	0.085	1.12	1.04	0.79	0.051	1.04
S	Ba	8	−98.8	1.72	1.00	0.098	1.06	1.03	0.78	0.059	0.98
S	K	14.5	−136.3	1.59	0.96	0.075	1.12	0.95	0.76	0.045	1.04
S	Ba	14.5	−112.5	1.61	0.96	0.084	1.08	0.96	0.76	0.050	1.00
S	K	16	−127.6	1.52	0.94	0.072	1.10	0.91	0.74	0.043	1.03
S	K	21	−156.3	1.53	0.94	0.066	1.14	0.91	0.74	0.039	1.06
S	Ba	21	−109.6	1.68	0.98	0.090	1.08	1.00	0.78	0.054	1.00
C	Ba	5	−148.4	1.64	0.97	0.075	1.13	0.98	0.77	0.045	1.05
C-0.75	K	8.5	−116.7	1.77	1.01	0.095	1.09	1.06	0.80	0.057	1.01
C-0.95	K	8.5	−96.5	1.75	1.01	0.102	1.05	1.05	0.79	0.061	0.98
C-1.20	K	8.5	−113.4	1.70	0.99	0.091	1.08	1.02	0.78	0.054	1.01
C-1.50	K	8.5	−95.4	1.75	1.01	0.103	1.05	1.05	0.79	0.062	0.98
C	Ba	8.5	−110.8	1.75	1.00	0.095	1.08	1.04	0.79	0.057	1.00
C	Ba	15	−133.1	1.73	1.00	0.086	1.11	1.03	0.79	0.051	1.03

(−113.09) or tetrahedral (−70.72) ionic aggregates. In the previous section, the cubic model has been mentioned and the cube edge has been approximated to 3.3 Å in agreement with a previous study.[34] The volume of cubic aggregates should thus be very small and the number of cations as well. This model is not consistent with a well-defined and intense ionic peak. Although it has the same angulosity as a cube, a parallelipipedon leads to a smaller ρ_0 (<0) value and does not accordingly improve the results. Furthermore, a cubic aggregate exhibits parallel interfaces which should produce oscillations in the tail end of the SAXS intensity. Such oscillations are not observed. In contrast, tetrahedron does not give oscillations due to the absence of parallel faces.

Table 5 reports the side a_s of a tetrahedron as approximated from $K_6/K_P(\Theta/S)$. From $K_P/Q(S/V_2)$, another estimation of the side of the terahedron is obtained, i.e., a_v. The a_s/a_v ratio (Table 5) is close to 1 which gives coherence to the model. The side of the tetrahedron is approximately equal to 9−10 Å and its volume is on the order of $k_v a^3 \approx 90$ Å^3. Since the cation volume may vary from 3.5 Å^3 (Ca, Na) to 19.5 Å^3 (Cs), the ionic aggregates would contain a few cations. The surface S and the volume V of tetrahedral ionic aggregates are listed in Table 5. Figure 12a illustrates a tetrahedric aggregation model for the cations. Six spherical cations form an equilateral prism, the cavity of which contains three extra cations, and the top is capped by a tenth cation. The tetrahedron, which contains 10 cations, must of course be surrounded by the anions as schematized in Figure 12b. The four cations situated at the vertexes of the tetrahedron are surronded by three cations and four anions while the cations situated at the middle of the edges of the tetrahedron are surrounded by six cations and seven anions. The orbital electron of the metal is moved toward the outside of the tetrahedron and the electrostatic configuration of the model results in 10 dipoles, the positive charges being located near the external surface of the tetrahedron. The distance between two next-neighboor positive charge corresponds to the half-side of the tetrahedron, i.e., on the order of 0.5 nm (Table 5). The electrostatic repulsion between the positive charges is very small. The orientation of the dipoles is equivalent to the organization of 10 identical dipoles in a radial electrostatic field pointing to to the center of the tetrahedron. The suggested configuration corresponds to the ideal spatial orientation in the case of a locally isotropic electrostatic radial field. Admitting that n PIP chain ends are concentrated in a small region, the negative charges of sulfonate (or carboxylate)

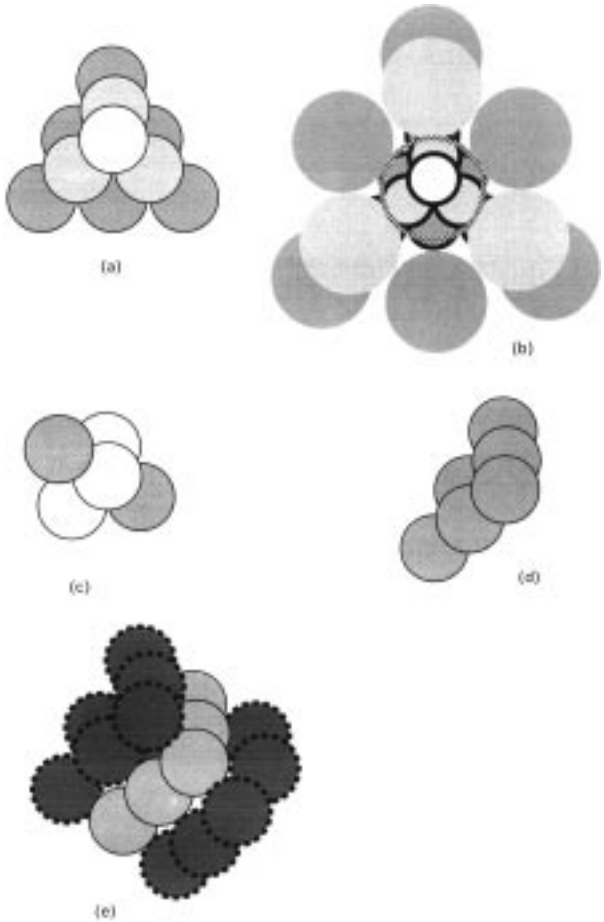

Figure 12. Sketch of the ionic aggregates according to the tetrahedral model (a), the hexahedral model (c) and the prismatic model (d). Parts b and e extend parts a and c to the aggregation of the anionic chains.

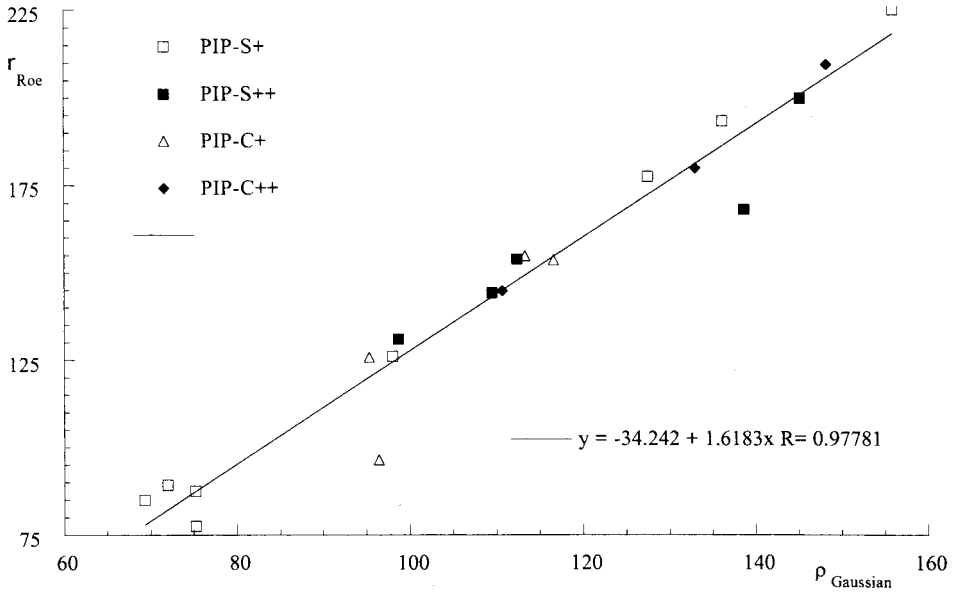

Figure 13. Plot of ρ_{Roe} vs ρ_{Gauss} for each type of telechelic PIP considered in this study.

anions produce an electrostatic fields oriented toward the center of the chain end distribution. The cations are forced to enter in the inner sphere defined by the negative shell of the oxygens. The electrostatic configuration corresponds to a negative shell containing n positive charges which organize themselves so that repulsive electrostatic energy will be minimum. Positive charges are located in the vicinity of the negative shell and the distance between them (0.5 nm) is large so that repulsive energy is very small. The organization of the cations within the negative shell would be of the hexagonal compact or cubic type, as in metal or inert gas crystals. However, the limited number of cations does not promote this type of structure which is encountered in a lattice with a great number of atoms. Tetrahedral organization is not fundamentally different from the hcp or fcc cubic structure but it develops a closed structure due to the limited number of atoms while hcp and fcc develops open structure using the binding cohesion between atoms of adjacents cells within the lattice. The thickness of the interphase, $E = 12^{1/2}\sigma$, is on the order of the oxygen diameter as can be seen from Table 2. The volume of this negative region around the cationic tetrahedron is consistent with the volume of 10 anions.

An extension of this model for monovalent cations to the bivalent cations requires to accommodate five cations for 10 anions. A hexahedron consisting of two tetrahedrons with a common face (Figure 12c) is not acceptable because the theoretical value for $\rho_0 = -607$ ($\Theta_0 = -0.52$) does not agree with ρ_{exp}. From the first plane of the tetrahedron (Figure 12d), a triangular prism of six cations may be considered, the height of which is the cation diameter. Then $\Theta_0 = -3.16$ and $\rho_0 = -109.32$ which is in very good agreement with ρ_{exp}. Table 5 reports the calculated a_s and a_s/a_v values for this model. The maximum relative discrepancy is only 7%. The ionic aggregate dimension, a, is approximately 0.75 nm. This aggregate structure is consistent with cations binding two chains (anions) as shown in Figure 12e. The broadness of the transition zone between the cationic and the polymeric phases matches the anion dimension.

If r is the cation radius, the side of the tetrahedron is $2r\,(2 + 6^{1/2}) \approx 8.9r$ and the side of the equilateral prism is $2r(2 + 3^{1/2}) \approx 7.5r$. The external surface S and volume V are $137.2r^2$ and $83.1r^3$, respectively, for the tetrahedron and $93.0r^2$ and $48.2r^3$ for the equilateral prism. It can be checked that calculated surfaces and volumes (Table 5) are consistent with r that ranges from 0.9 to 1.3 Å.

The general discussion about the form of the ionic aggregates is supported by the data resulting from the analysis of the transition zone between the phases with a Gaussian profile. If the Roe profile is considered, the S/V ratios must be increased by 20% (eq 17). As S results from K_6/K_P, which does depend on the function G or R, V must be 20% smaller in case of the Roe function (Figure 13). Then a_v is decreased by 6%, and the ratio a_s/a_v is increased by 6% and is in the range of 1.02−1.21 for monovalent cations and 1.05−1.11 for divalent cations. Thus, the Roe profile also agrees very well with the two proposed models.

The results in Table 5 show that a, S, and V increase with r, whereas they are largely independent of the anion, the PIP molecular weight, and the valency of the cation. S/V_2 is usually smaller for monovalent than for divalent cations in agreement with a larger volume for the tetrahedric aggregates proposed for the alkali-metal cations compared to the prismatic model which fits better the alkaline-earth-metal series.

Conclusions

Since the Bragg spacing (d_{IP}) is regularly increasing with the chain molecular weight (M_n), it is clear that an internodular interference is at the origin of the ionic peak observed for the investigated series of HTP's.

Consistently, the calculated distance, d_{IN}, between the near-neighbor nodules is the length of the polymeric chain which is in the unperturbed state or not, depending on the anion (sulfonate or carboxylate) and the polymer backbone. The cation and the extent of neutralization of the acid end groups have only a minor effect, since they appear to change merely the volume of the nodules. The shape and intensity of the ionic peak depends on both the anion and the cation, which is consistent with a "cationic" model in which the cations form ionic microphases surrounded by the anionic end groups that would be nothing but the interphase.

As far as additional although very weak scattering maxima are observed, their position with respect to the main peak agrees with an hexagonal organization of the ionic microphases. In this hexagonal chain network, the distance, d_{IN}, between two ionic nodules is 1.15 d_{IP}, and the degree of order is rather low. Indeed, the extension of the network must be limited in space, so that inhomogeneities of a characteristic size much larger than the internodule distance would exist and would be at the origin of the strong forward scattering observed in the HTP's.

The shape of the ionic aggregates has been approximated from the tail end analysis of the scattering curve. The ionic aggregates are proposed to be tetrahedric or prismatic depending on the cation valency (mono- or divalent). The tetrahedric aggregates are proposed to contain 10 monovalent cations, whereas six divalent cations would contribute to the prismatic ones. These shapes are largely independent of the sulfonate and carboxylate end groups.

Acknowledgment. R.S., F.F., and J.L. are very grateful to the Fonds National de la Recherche Scienntifique (FNRS) and to the Fonds de la Recherche Fondamentale Collective (FRFC) for subsidiation of a new equipment at University of Liège. R.J. is very much indebted to the "Services Fédéraux des Affaires Scientifiques, Techniques et Culturelles" for financial support in the frame of the "Pôles d'Attraction Interuniversitaires Polymères". M.F. thanks the "institut pour l'Encouragement de la Recherche Scientifique dans l'Indiustrie et l'Agriculture" (IRSIA) for a fellowship.

Supporting Information Available: Figures plotting pinhole intensity (in arbitrary units) vs s (nm^{-1}) for α,ω-barium sulfonato polyisoprenes (Figure D1) and α,ω-barium carboxylato polyisoprenes (Figure D2) (2 pages). Ordering and Internet access information is given on any current masthead page.

References and Notes

(1) Eisenberg, A. *Macromolecules* **1970**, *3*, 147.
(2) Mauritz, K. A. *J. Macromol Sci., Rev. Macromol. Chem. Phys.* **1988**, *C28*, 65.
(3) Eisenberg, A.; Hird, B.; Moore, R. B. *Macromolecules* **1990**, *23*, 4098.
(4) Gao Zh.; Zhong X.-F.; Eisenberg A., *Macromolecules* **1994**, *27*, 794.
(5) Vanhoorne P.; Jérôme R.; Teyssié P.; Laupêtre F. *Macromolecules* **1994**, *27*, 2548.
(6) Jérôme R. In *Telechelic Polymers: Synthesis and Applications*; Goethals, E. G. Ed.; CRC Press: Boca Raton, FL, 1989; Chapter 11.
(7) Ledent, J.; Fontaine, F.; Reynaers, H.; Jérôme, R. *Polym. Bull.* **1985**, *14*, 461.
(8) Williams, C. E.; Russel, T. P.; Jérôme, R.; Horrion, J. *Macromolecules* **1986,** *19*, 2877.
(9) McKnight, W., J.; Earnest, T. R., Jr. *J. Polym. Sci., Macromol. Rev.* **1981**, *16*, 41.
(10) Tant, M. R.; Wilkes, G. L. *J. Macromol. Sci., Rev. Macromol. Chem. Phys.* **1988**, *C28* (1), 1.
(11) Fitzgerald, J. J.; Weiss, R. A. *J. Macromol. Sci., Rev. Macromol. Chem. Phys.* **1988**, *C28* (1), 99.
(12) Yarusso, D. J.; Cooper, S. L. *Macromolecules* **1983**, *16*, 1871.
(13) Yarusso, D. J.; Cooper, S. L. *Polymer* **1985**, *26*, 371.
(14) Lee, D. C.; Register, R. A.; Yang, C. Z.; Cooper, S. L. *Macromolecules* **1988**, *21*, 998.
(15) Visser, S. A.; Cooper, S. L. *Macromolecules* **1991**, *24*, 2584.
(16) Meyer, C. T.; Pineri, M. *J. Polym. Sci., Polym. Phys. Ed.* **1978,** *16*, 569.
(17) Chu, B.; Wang, J.; Li, Y.; Peiffer, D. G. *Macromolecules* **1992**, *25*, 4229.
(18) Galambos, A. F.; Stockton, W. B.; Koberstein, J. T.; Sen, A.; Weiss, R. A.; Russel, T. P. *Macromolecules* **1987**, *20*, 3091.
(19) Chu, B.; Wu, D. Q.; MacKnight, W. J.; Wu, C.; Phillips, J. C.; Legrand, A.; Lantman, C. W.; Lundberg, R. D. *Macromolecules* **1988**, *21*, 523.
(20) Ding, Y. S.; Hubbard, S. R.; Hodgson, K. O.; Register, R. A.; Cooper, S. L. *Macromolecules* **1988,** *21*, 1698.
(21) Register, R. A.; Sen, A.; Weiss, R. A.; Cooper, S. L. *Macromolecules* **1989**, *22*, 2224.
(22) Wu, D. Q.; Phillips, J. C.; Lundberg, R. D.; MacKnight, W. J.; Chu, B. *Macromolecules* **1989**, *22*, 992.
(23) Jérôme, R. In *Structure and Properties of Ionomers*; Pineri, M., Eisenberg, A., Eds.; D. Reidel Publ. Co.: Dordrecht, The Netherlands, 1987; 399.
(24) Broze G.; Jérôme R.; Teyssié Ph., *Macromolecules* **1982**, *15*, 1920.
(25) Register, R. A.; Foucart, M.; Jérôme R.; Ding Y. S. ; Cooper S. L. *Macromolecules* **1988**, *21*, 1009.
(26) Vonk, C. G. *J. Appl. Crystallogr.* **1971**, *4*, 340.
(27) Sobry, R.; Rassel, Y.; Fontaine, F.; Ledent, J.; Liegeois, J.-M. *J. Appl. Crystallogr.* **1991**, *24*, 692.
(28) Koberstein, J. T.; Morra, B.; Stein, R. S. *J. Appl. Crystallogr.* **1980**, *13*, 34.
(29) Vonk, C. G. *J. Appl. Crystallogr.* **1973**, *6*, 81.
(30) Bonart, H.; Muler, E. H. *J. Macromol. Sci. Phys.* **1974**, *B10*, 177.
(31) Roe, R. J. *J. Appl. Crystallogr.* **1982**, *15*, 182.
(32) Ciccariello, S. *Phys. Rev. A* **1991**, *44*, 2975.
(33) Kirste, R.; Porod, G. *Kolloid Z.* **1962**, *184*, 1.
(34) Sobry, R.; Ledent, J.; Fontaine, F. *J. Appl. Crystallogr.* **1991**, *24*, 516.
(35) Sobry, R.; Fontaine F.; Ledent, *J. Appl. Crystallogr.* **1994**, *27*, 482.
(36) Méring J.;Tchoubar, D. *J. Appl. Crystallogr.* **1968**, *1*, 153.
(37) Ciccariello, S.; Sobry, R. *Acta Crystallogr.* **1995**, *A51*, 60.
(38) Ciccariello, S.; Sobry, R. To be published in *J. Appl. Crystallogr.*
(39) Todo, A.; Hashimoto, T.; Kawai, H. *J. Appl. Crystallogr.* **1978**, *11*, 558.
(40) Soler, J.; Baldrian, J. *J. Appl. Crystallogr.* **1972**, *5*, 428.
(41) Young, R. J.; Lovell, P. A. *Introduction to polymers*; Chapman & Hall: New York, 1991; Chapter 3.
(42) Fontaine, F.; Ledent, J.; Sobry R.; François E.; Jérôme R.; Teyssié, P. *Macromolecules* **1993**, *26*, 1480.
(43) Maus, C.; Fontaine F.; Van den Bossche G.; Sobry, R.; Jérôme, R. *J. Phys. IV* **1993**, *3*, C8, Suppl. JP III, 12.

MA970065V